NUCL SCI TECH (2022) 33:121
https://doi.org/10.1007/s41365-022-01104-z

Discussion of 90° stopband in low-energy superconducting linear accelerators

Xin-Miao Wan[1] · Xue-Jiang Pu[1] · Zhi-Qiang Ren[1] · Wei-Hong Huang[1] · Yu-Fei Yang[1] · Zhi-Hui Li[1]

Received: 3 April 2022 / Revised: 11 July 2022 / Accepted: 16 July 2022 / Published online: 24 September 2022

Abstract Superconducting linear accelerators (SCL) have a high acceleration gradient and are capable of operating in a high-duty factor mode. For high-power and high-intensity SCL, the design of beam dynamics generally follows the principle that the zero-current periodic phase advance (σ_0) of each degree of freedom is less than 90° to avoid envelope instability caused by space charge. However, this principle is obtained under the condition of a completely periodic focusing channel, and it is ambiguous for pseudo-periodic structures, such as linear accelerators. Although transverse beam dynamics without acceleration have been studied by other researchers, it appears that there are some connections between pure 2D and 3D beam dynamics. Based on these two points, five focusing schemes for the solenoid and quadrupole doublet channels were designed to simulate the beam behavior with non-constant σ_0. Among them, the four schemes follow the characteristics of variation in the zero-current longitudinal phase advance (σ_{0l}) under a constant acceleration gradient and synchronous phase. The zero-current transverse phase advance (σ_{0t}) is consistent with σ_{0l}, based on the equipartition requirement. The initial σ_{0t} was set to 120°, 110°, 100°, and 90°, and was then gradually decreased to approximately 40° at the end of the channel. The last scheme maintains the maximum σ_{0t} of 88° by reducing the acceleration gradient of the corresponding cavities, until the point at which σ_{0t} equals 88° with a normal gradient. Using the stopbands obtained from the linearized envelope equations and multiparticle particle-in-cell (PIC) simulations, the transport properties of both continuous and 3D-bunched beams with the acceleration of the five focusing schemes were studied. It was found that for a CW beam, when tune depression > 0.7, σ_{0t} can break through 90° when the beams were transported in both solenoid and quadrupole doublet periodic focusing channels. When tune depression < 0.7, the conclusions were different. For the solenoid focusing system, σ_{0t} can partially break through 90°, and the beam quality is not significantly affected. For the quadrupole doublet focusing system, a partial breakthrough of 90° has a greater impact on the beam quality. The same conclusions were obtained for a bunched beam with acceleration.

Keywords Proton beam · Superconducting linear accelerators · Envelope instability · Periodic focusing structure · Resonance

This study was supported by the National Natural Science Foundation of China (Nos. 11375122 and 11875197).

✉ Zhi-Hui Li
lizhihui@scu.edu.cn

[1] The Key Laboratory of Radiation Physics and Technology of Ministry of Education, Institute of Nuclear Science and Technology, Sichuan University, Chengdu 610065, China

1 Introduction

Linear accelerators (linacs) have been investigated for several applications [1]. Since the successful first operation of a particle accelerator at the beginning of the last century, remarkable advances have been made in the physics and technology of linacs [2]. Theoretical and experimental studies on the stability of high-intensity beams in linacs began in the 1960s. Most of these theoretical studies have been based on two-dimensional transport models without acceleration [3]. The associated strong space-charge effects present challenges in the transport of high-intensity beams

[4]. One of the conclusions of these studies is that when transverse phase advance per period σ_{0t} is greater than 90°, the space charge force may drive envelope instability and degrade the beam quality [5, 6]. To avoid envelope instability in high-intensity linacs, one of the rules that most designers follow is to maintain $\sigma_{0t} < 90°$ [7]. When the phase advance is near 90°, fourth-order resonance and envelope instability occur [8]. The first experimental study of the fourth-order resonance in an operational high-intensity accelerator was undertaken at GSI UNILAC, which confirmed the emittance degradation [9]. For Kapchinskij-Vladmirskij (K-V) beams, using perturbation analysis of the linearized Vlasov–Poisson equations, stopbands of instability can be obtained [5]. Stopbands are defined as regions in which any eigenvalue lies outside the complex unit cycle. In stopbands, the emittance increases exponentially in a nonzero state. Higher-order and lower-order stopbands may coincide, but instability typically decreases with increasing order [10]. Meanwhile, the special case of the "second-order even" mode is known as the envelope instability [11]. Envelope instability is characterized by parametric and confluent resonance. Parametric resonance represents the resonance between the focusing lattices and one of the envelope oscillatory modes that occurs only in the solenoid channel. When parametric resonance occurs, only one of the breathing and quadrupole modes excites resonance with the beam core. This is also called half-integer resonance because it represents the envelope eigenmode that oscillates at half the frequency of the periodically varying focusing (including space charge). Confluent resonance represents the resonance between both envelope oscillation modes and lattices, which occurs only in the quadrupole channel [12].

The space charge force not only causes envelope instability, but may also cause coupling of the particle motions and emittance exchange in different directions [13]. Therefore, Jameson introduced the equipartition concept into the beam dynamics design of linear accelerators [9, 14]. By properly setting the longitudinal and transverse focusing strengths, the oscillation energies of different degrees of freedom were balanced, and there was no free energy for resonance to occur. For the equipartition design, the motions of the particles in the transverse and longitudinal directions are decoupled. Therefore, the transverse and longitudinal motions of the superconducting linear accelerator (SCL) based on equipartition design can be studied separately. However, σ_{0t} and σ_{0l} maintain the same trend because of the requirement for equipartition.

SCL can provide high-power beams and have many applications in various fields. It has negligible wall power losses, which makes it possible to operate in the high-duty factor mode with a higher accelerating gradient. The SCL is typically composed of different acceleration sections, and each section is composed of identical cells [15]. The significant difference between SCL and periodic focusing channels is that SCL have radio-frequency (RF) cavities. The RF cavity can not only accelerate beams, but can also provide focusing in the longitudinal direction and defocusing in the transverse direction to the particles [16]. One of the most important outcomes for the SCL is the pseudo-periodic focusing structure, which may lead to different dynamics. When the acceleration gradient and synchronous phase are constant, the square of the focusing strength is inversely proportional to the 3D power of the $\beta\gamma$ of particles [17]

$$\sigma_{0l}^2 = \frac{2\pi q E_0 T S^2 \sin(-\phi_s)}{mc^2 \beta_s^3 \gamma_s^3 \lambda}. \tag{1}$$

Thus, the maximum σ_{0l} occurs at the beginning of each section and decreases as the beam energy increases with the SCL. However, cavities at the beginning of each section must work under a reduced acceleration gradient because of the principle that $\sigma_0 < 90°$. This significantly reduces the acceleration efficiency.

The remainder of this paper is as follows. In Sect. 2, five different focusing schemes are designed and presented. In Sect. 3, the types and characteristics of periodic focusing channels and an approach for calculating the stopbands are introduced in detail. In Sect. 4, the beam dynamics of five different focusing schemes are shown. Finally, the effects of σ_{0l} exceeding 90° in a real SCL section are studied and verified. The conclusions and discussion are presented in Sect. 6.

2 Different focusing schemes

To study the transverse beam dynamics when σ_0 partially exceeds 90°, five different focusing schemes were designed to simulate σ_{0t}. The maximum σ_{0t} of the beam was designed to be 120° (①), 110° (②), 100° (③), and 90° (④). The purpose was to simulate the trend of σ_{0t} under different acceleration gradients in the presence of an acceleration field. A higher acceleration gradient corresponds to a larger σ_{0t}. The first scheme corresponds to the highest acceleration gradient and the fourth scheme corresponds to the lowest acceleration gradient. To avoid excessive sensitivity of the beam to the focusing parameters, for every focusing scheme, the minimum value of σ_{0t} was generally set to 40° after the beam passes through 80 focusing periods. Therefore, we designed focusing schemes based on a logistic function. This function is more suitable for the changes in σ_{0t}. In addition, for the case in which the maximal σ_{0t} was 120°, a control scheme was set to avoid envelope instability on the beam. The maximal σ_{0t}

of this control scheme was 88° (⑤), where envelope instability does not occur. This can be controlled by reducing the acceleration gradient of the corresponding cavity. Once σ_{0t} of ① was less than 90°, ⑤ and ① remain within the same gradient. The common logistic function is given by

$$y = A_2 + \frac{A_1 - A_2}{1 + \left(\frac{x}{x_0}\right)^p}. \quad (2)$$

In the design functions, x represents the period number, and y represents the value of σ_{0t}. The specific parameters of the functions are listed in Table 1. Additionally, σ_{0t} of the five schemes are shown in Fig. 2.

3 The focusing channels and stopbands

3.1 Periodic focusing channels

According to the transverse motion equation, the RF electromagnetic field has an evident defocusing effect and axial symmetry at the low-energy end of the linear accelerator. Considering that the beam has a strong space-charge effect at the low-energy end, a relatively compact transverse focusing lattice is required to maintain an appropriate beam size within our design. Magnetic quadrupoles, solenoids, and axisymmetric electrostatic lattices were chosen by designers for beam transport systems at low-energy ends [18]. In this study, a solenoid, which has axial symmetry, and a quadrupole doublet, which is non-axisymmetric, were chosen as the focusing elements. The specific parameters of the focusing elements used for the following discussion are shown in Fig. 1. For the solenoid periodic focusing system, the $\kappa(s)$ is given by [12]

$$\kappa(s) = \kappa_x(s) = \kappa_y(s) = \left[\frac{qB}{2m_0 c\beta\gamma}\right]^2, \quad (3)$$

where B is the solenoid lens strength. For a magnetic quadrupole channel,

$$\kappa(s) = \kappa_x(s) = -\kappa_y(s) = \frac{G}{m_0 c\beta\gamma}, \quad (4)$$

where G is the quadrupole linear strength gradient.

The distribution of beam particles in phase space plays a significant role because it is directly related to the space charge in high-intensity proton accelerators. The *K-V* distribution is an ellipse with uniform density in any projected phase plane, which is beneficial for calculating the space charge force. This is because the space charge force is a linear defocusing force that can be compensated for by an external field. Therefore, the *K-V* distribution is most commonly used for researching space charges in simulations.

From the research of Sacher, the exact form of the distribution hardly works on the linear part of the self-field, while the RMS size of the distribution plays an important role. The envelope equations can be used directly in simulations when there is little variability in the distribution during beam transport. Simultaneously, the results of previous research have shown that beams with different distributions but with the same beam emittance terms can be equivalently considered [19]. Generally, it is justified to use the results from the *K-V* distribution for the other beam distributions.

When particles are randomly generated in the *K-V* transverse ellipsoid, the envelopes where $X(s)$ and $Y(s)$ are in the two transverse directions of the periodic focusing channels are described by [12]

$$X'' + \kappa_x(s) \cdot X - \frac{\varepsilon^2}{X^3} - \frac{2K}{X+Y} = 0, \quad (5)$$

$$Y'' + \kappa_y(s) \cdot Y - \frac{\varepsilon^2}{Y^3} - \frac{2K}{X+Y} = 0, \quad (6)$$

where $K = 2eI/4\pi\varepsilon_0 mc^3\beta^3\gamma^3$ is the generalized provenance. Meanwhile, $\kappa_x(s)$ and $\kappa_y(s)$ represent the transverse focusing functions, and $\varepsilon = \varepsilon_x = \varepsilon_y$ during beam transport.

3.2 Calculating the stopbands

The mismatch between the periodic focusing channels and particles can cause envelope resonance. This is an important factor in space-charge-dominated beams. At present, there are several methods for calculating envelope instability stopbands caused by resonance. First, using the theory established by Struckmeier and Reiser, it is solved by linearizing differential equations with disturbance terms [11]. Second, the perturbation theory based on the Chernin matrix can also obtain a complete set of second-order

Table 1 The specific parameters of logistic functions for σ_{0t}

Scheme	Max σ_{0t} (°)	Min σ_{0t} (°)	A_1	A_2	x_0	p
①	120	40	120	29.8312	26.3333	1.87755
②	110	40	110	31.1023	26.3333	1.87755
③	100	40	100	32.3734	26.3333	1.87755
④	90	40	90	33.6445	26.3333	1.87755

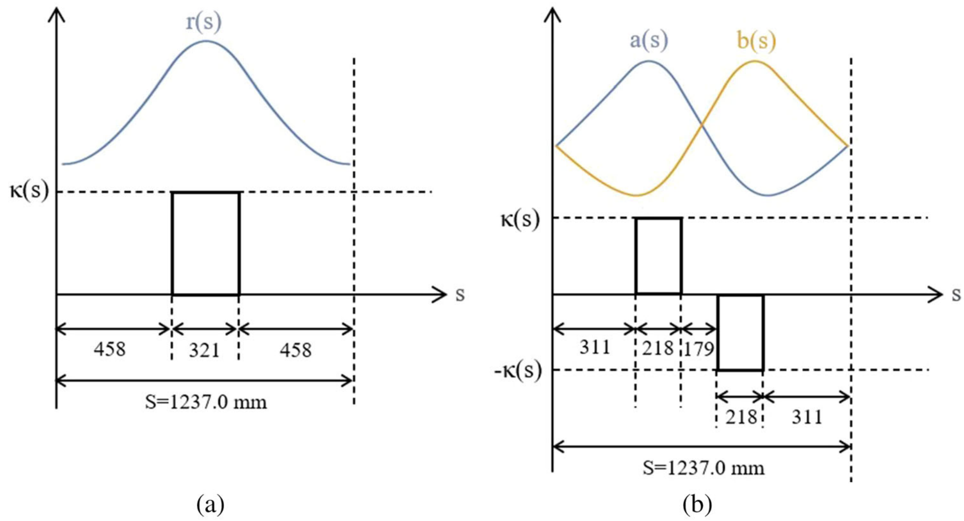

Fig. 1 Periodic focusing elements and the corresponding matched beam envelopes. **a** Solenoid, **b** quadrupole doublet. The length of each element is 1237.0 mm

instabilities, including even and odd modes. The sum effects of the resonance on the beam were also analyzed [20]. Finally, perturbation theory based on the Vlasov–Poisson equations introduced by Hofmann provides an approach for calculating the stopbands of higher-order perturbations [5]. Because the perturbation theory established by Struckmeier and Reiser is relatively mature, widely used, and highly reliable, envelope instability stopbands are calculated based on this theory.

With $z = (x, x', y, y')$, an ensemble of phase space trajectories is represented which satisfies $Z(s+S) = M(s)Z(s)$ in a periodic dynamics system. It is useful to define $M(s)$ as the transfer matrix, where $M(s) = M(s+S)$ is also satisfied in a periodic dynamics system. Overall, λ denotes the eigenvalues of the transfer matrix that can be greater than 1 or less than 1. If $|\lambda| = 1$, the system is stable; otherwise, the system is unstable. Meanwhile, λ satisfies $\lambda = |\lambda| e^{i\phi}$, where ϕ represents the eigenphase $Arg[M(s)]$ of the transfer matrix. Additionally, ϕ connects with the envelope modes [21]. Finally, by converting ϕ to σ, a stopband with a specific σ_{0t} can be obtained under a certain focusing structure.

Since σ_{0t} is different in each period, different values of σ_{0t} corresponds to different stopbands. Therefore, we need to separately calculate the stopbands corresponding to different σ_{0t} values and summarize the results. Finally, the stopbands that change with the period can be obtained using Mathematica, as shown in Fig. 2 [22]. Because σ_{0t} of schemes ④ and ⑤ are designed to be less than or equal to 90°, there are no stopbands. Hence, this is not shown within this paper. Here, $\sigma_t = \frac{\sigma_x + \sigma_y}{2}$, which represents an isotropic beam.

4 Simulation results of beam evolution under different focusing schemes

TraceWin conducts simulations of any initial beam distribution and three-dimensional space charge force tracking simulation with a wonderful accelerator design capability; therefore, TraceWin was chosen for our simulation [23]. PARTRAN was used for multi-particle simulation and tracking. Subsequently, the *K-V* distribution was selected because it has many advantages in analyzing the effect of space charge. The initial kinetic energy of the proton beam was 10 MeV. The initial normalized RMS emittance of the CW beam was set to be 0.2 π mm mrad in both the *x-x*' and *y-y*' planes. The number of particles was set as 100,000. σ_{0t} follows a focusing scheme. It is well established that a tune depression of 0.71 represents a dividing line. When the tune depression is greater than 0.71, the beam is dominated by the emittance. When the tune depression is less than 0.71, the beam is dominated by space charge [24]. Accordingly, the range of tune depression values was chosen from 1.0 to 0.6 to ensure a simulation that adapted well to various situations. By setting the initial conditions, the beam dynamics were simulated using TraceWin code. Here, we mainly discuss the parameters related to the beam quality, such as the RMS emittance and the particle distribution in the phase space. The normalized RMS emittance $\varepsilon = \frac{\varepsilon_x + \varepsilon_y}{2}$ is defined because there is not much difference between ε_x and ε_y which can also effectively reduce the errors caused by the software calculations. Finally, the ε of the output during beam transport was obtained, as shown in Fig. 3.

It is clear that there are significant differences in ε between the quadrupole doublet and solenoid focusing channels. For the quadrupole doublet channels, when tune depression 0.7 and 0.6, the ε of focusing scheme ①

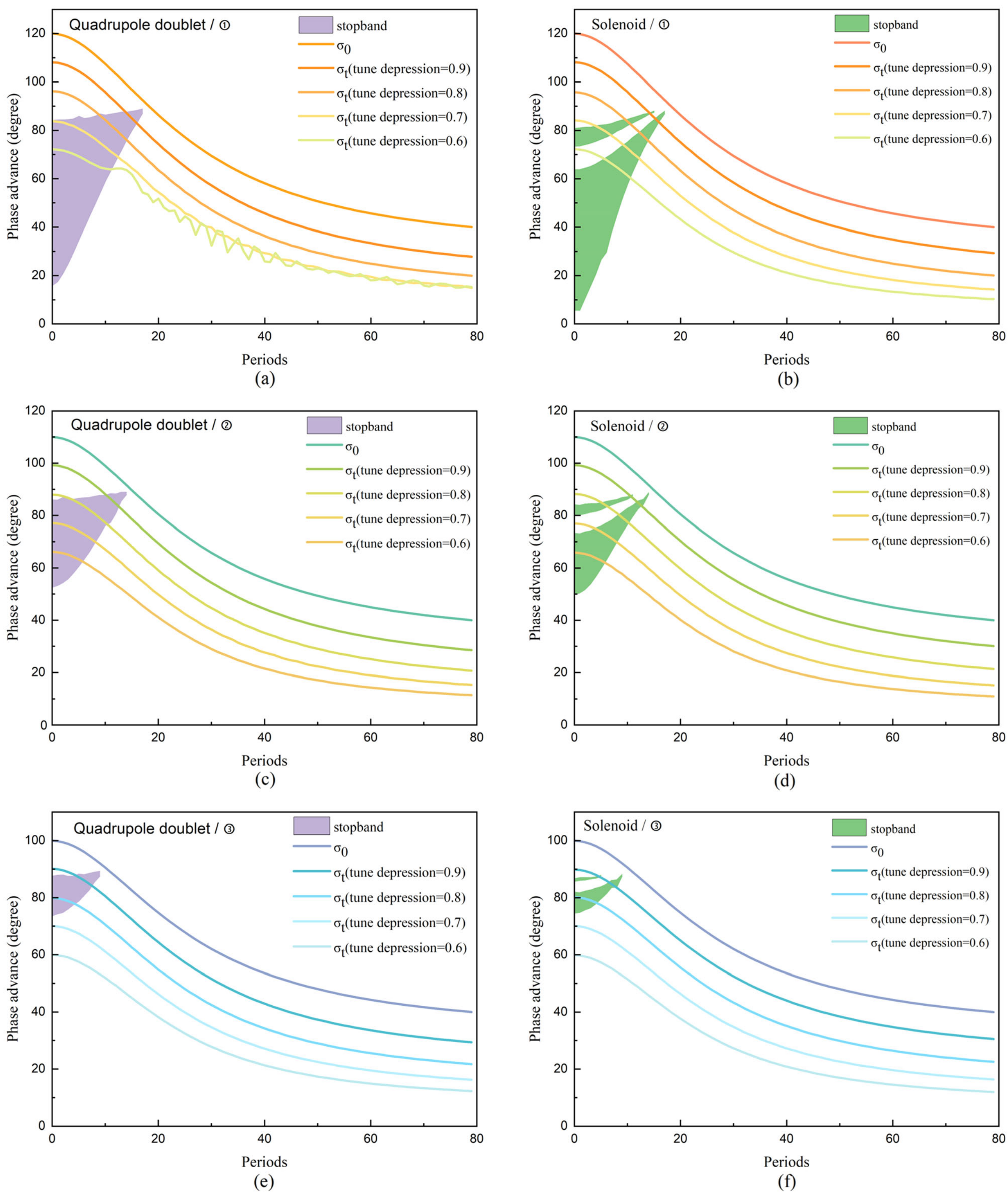

Fig. 2 (Color online) The stopbands correspond to different focusing schemes and different periodic channels. Each picture shows the change of beam σ_t under different tune depressions

increased significantly, while the beam designed by other focusing schemes exhibited no such behavior. For the solenoid channels, the tune depression and focusing schemes seem to have no significant effect on the beam quality. This shows that the beam quality can be improved using a periodic focusing solenoid channel.

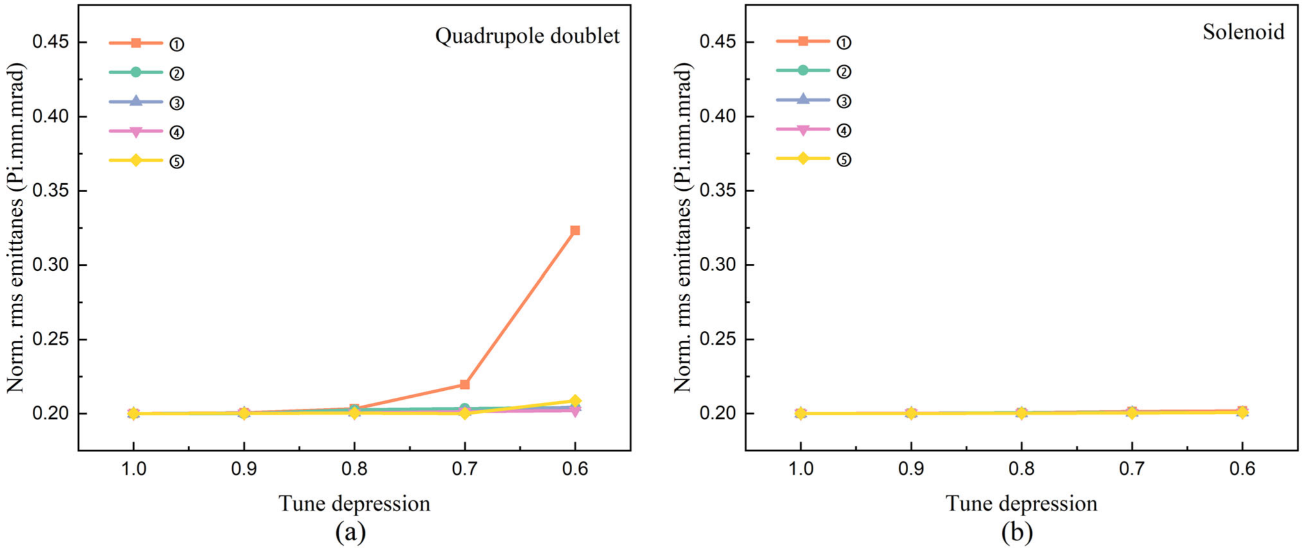

Fig. 3 (Color online) The ε when tune depression was equal to 1.0, 0.9, 0.8, 0.7, and 0.6 for different focusing schemes, respectively. **a** shows the results when the beams are transported in periodic focusing quadrupole doublet channels, and **b** shows the results when beams are transported in a periodic focusing solenoid channel

This can be explained as follows. It can be seen from Fig. 2 that the reduction speed of σ is consistent with σ_{0t}; beams transported in the solenoid channel take less time to cross the stopbands under the same focusing scheme and tune depression. With the enhancement of the space charge effect and the increase in the maximum value of σ_{0t}, this phenomenon becomes more obvious. In stopbands, the beams are affected by envelope instability, which deteriorates the beam quality. Moreover, most of the beams transported in the solenoid channels do not enter the stopbands at the beginning. This implies that the beam is less affected by the initial state.

Second, from previous studies by other researchers, envelope instability is caused by linearized perturbed oscillations of the breathing mode and quadrupole mode. The perturbations of the beam envelope are in phase when the breathing mode occurs, whereas out-of-phase perturbations of the beam exist when the quadrupole mode occurs. Parametric resonance can occur only in the breathing mode or quadrupole mode. Certainly, there is another type of resonance, called confluent resonance. Confluent resonance occurs when the two modes occur simultaneously. Confluent resonance means that the resonance effect is between the two envelope modes and focusing lattice. In a solenoid focusing channel, only one breathing or quadrupole mode can occur. This also means that, for a beam propagating in a solenoid, only parametric resonances cause instability. Meanwhile, the decoupling of the breathing and quadrupole modes means that the stopbands of parametric resonance for the two modes do not overlap. In contrast, in a quadrupole doublet focusing channel, only confluent resonance occurs, which involves locking of the breathing and quadrupole modes. The breathing and quadrupole modes are closely related and cannot be strictly separated [25]. If one mode is activated, the other is activated, which can result in a larger emittance. Third, compared to a solenoid channel, in a quadrupole doublet channel, the high-order stopbands overlap more with the envelope instability stopband, which can lead to an increase in emittance.

From Fig. 3a, it can be seen that when tune depression equals 0.7 or 0.6, the ε corresponding to focus scheme ① reaches a maximum, and when tune depression equals 0.6, ε has exceeded 10% of the initial emittance. To analyze this, particle distribution diagrams when beams were transported in the quadrupole doublet focusing channel with different tuning depressions are shown in Fig. 4. Simultaneously, relevant information about the beam transported in the solenoid focusing channel when the tune depression is equal to 0.6 is shown in Fig. 5, corresponding to focusing scheme ①.

From Fig. 4, it is clear that there is a four-fold structure and envelope instability structure in the phase space distribution of the particles, and there is an obvious growth in ε when the tune depression is equal to 0.6. The appearance of these structures is mainly due to the fourth-order resonance and envelope instability. Along with the beam envelope transport, envelope instability is excited from the mismatch generated by the fourth-order resonance [26]. Moreover, the fourth-order resonance appears earlier than the envelope instability. This also means that the fourth-order resonance stopband has some overlapping regions with an envelope instability stopband. Furthermore, as shown in Fig. 2a, the beam envelope enters the envelope

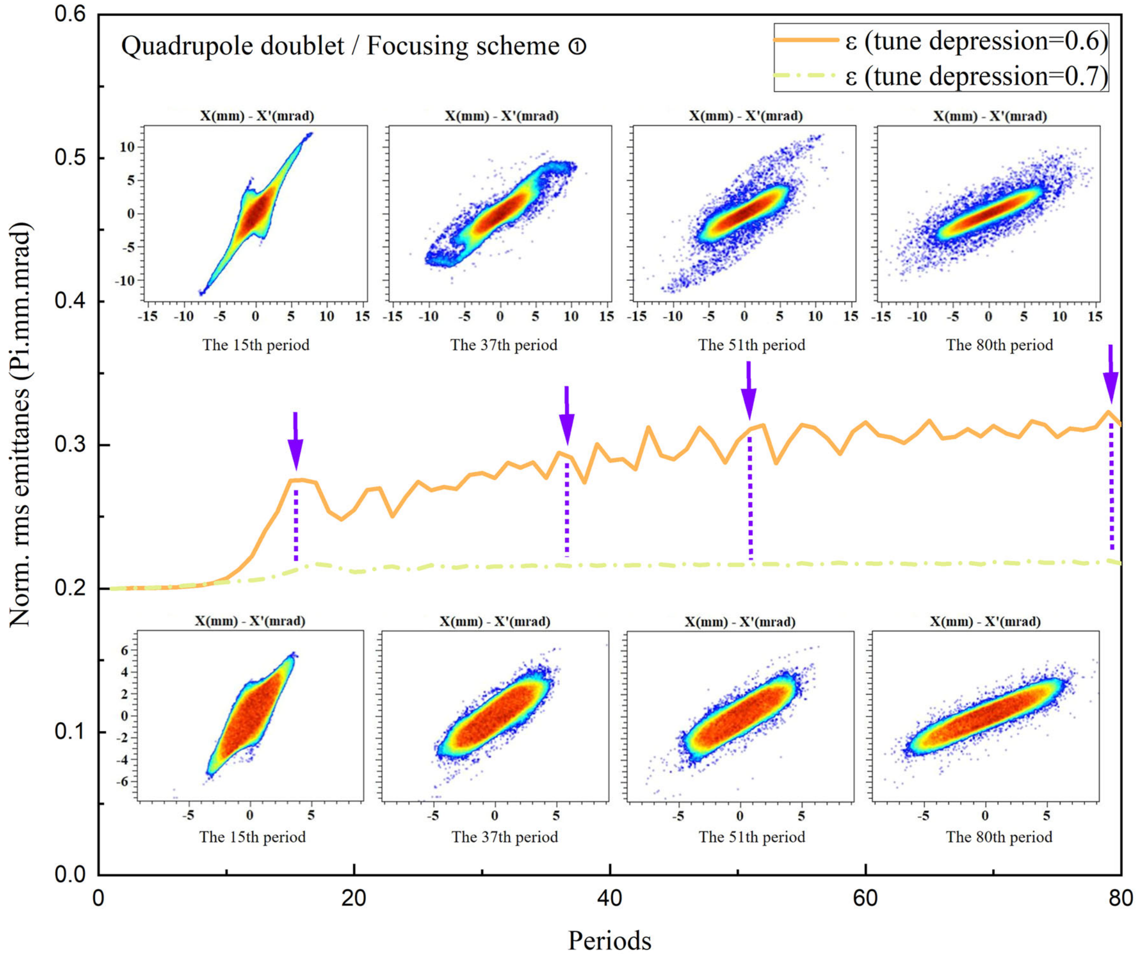

Fig. 4 (Color online) The ε and phase space distribution evolution along a quadrupole doublet channel under the focusing scheme ① when tune depression is equal to 0.6 and 0.7, respectively. Here, the particle distribution diagrams of the 15th, 37th, 51st, and 80th periods are shown

instability stopband for a relatively long time in the beginning when the tune depression is equal to 0.7 and 0.6, respectively. Hence, it is easy to observe an unstable structure in the phase–space distribution of the particles. In addition, as shown in Fig. 2, with a tune depression equal to 0.6, the beam takes more time to cross through the stopband. It seems that the stopband has a longer time to attract the beam owing to the space-charge effect. This further increased the emittance. As for the case in which the tune depression was equal to 0.7, in the first 20 periods, the distribution of particles in the phase space shows a four-fold structure. Hence, there is also a small increase in the emittance. The fourth-order resonance of the particle does not cause instability in the beam envelope, and the stopband has no obvious attraction to the beam. Finally, we analyzed the dynamics of the beam in the solenoid channel, as shown in Fig. 5. It is clear that the emittance does not exhibit a significant growth, regardless of the value of the tune depression and the scheme of focusing. Only the distribution of the particles in the phase space was elongated.

5 Simulation results of beam evolution with acceleration

The above simulation results are all obtained using pure 2D transverse dynamics, which do not consider acceleration. The beam dynamics when σ_{0t} locally exceeds 90° under acceleration are ambiguous. In this section, we consider 3D beam dynamics and simulate the evolution of the beam under acceleration. To explore this, we assumed two periodic acceleration channels, where each period element contains, for example, focusing lattices and acceleration structures, as shown schematically in Fig. 6. The length of each periodic element was 1236.0 mm, which is similar to that of the periodic element shown in Fig. 1.

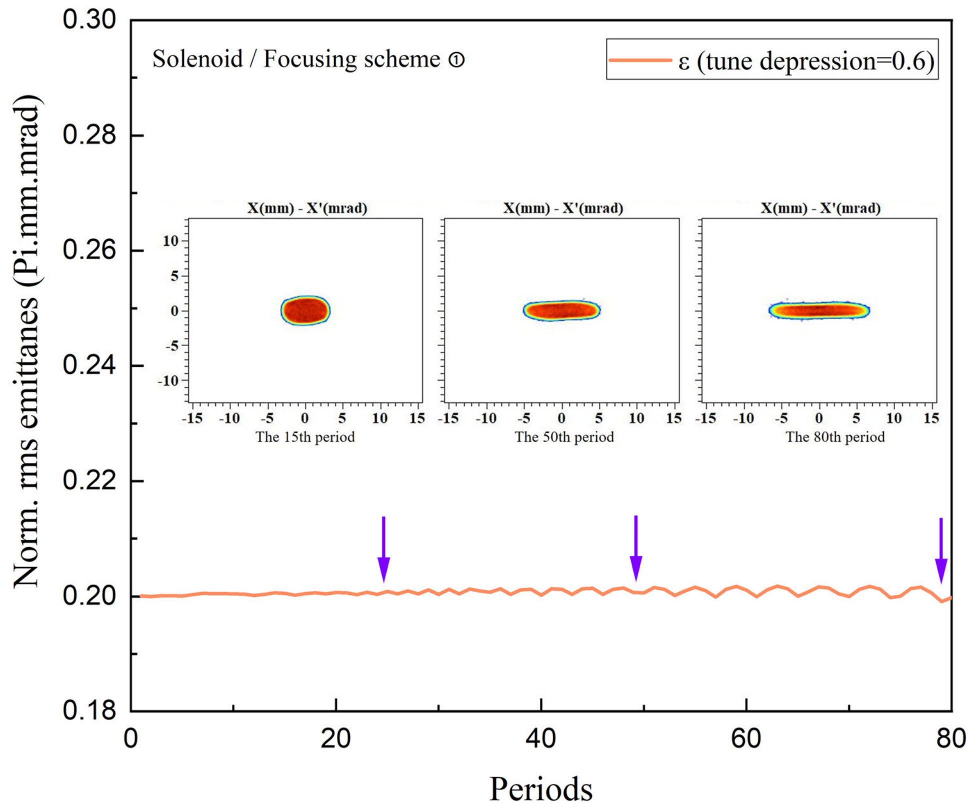

Fig. 5 (Color online) The ε and phase space distribution evolution along a solenoid channel under the focusing scheme ① when tune depression is equal to 0.6. Here, the particle distribution diagrams of the 15th, 50th, and 80th periods are shown

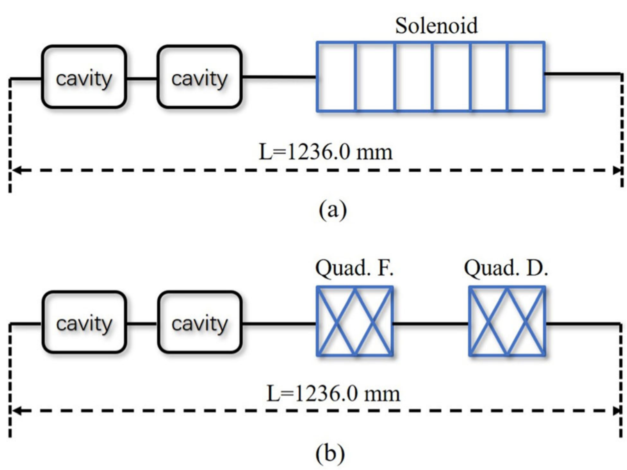

Fig. 6 Schematic plots of two periodic acceleration channels. **a** Shows the periodic element when beams are focused by solenoid lattice, and **b** shows periodic element when beams are focused by quadrupole lattice. The length of each cavity was 200.0 mm

To avoid coupling resonance between different degrees of freedom, it is necessary to optimize the selection of dynamic parameters using equipartition theory, so that the beam oscillation energy is balanced [27]. Under the condition of equipartition, σ_{0l} and σ_{0t} not only maintained the same changing trend but also satisfied $\frac{\varepsilon_{ln}}{\varepsilon_{tn}} = \frac{\sigma_t}{\sigma_l}$. Therefore, we assume that the maximum value of σ_{0l} is 2/3 of the maximum value of σ_{0t}. It is worth noting that σ_{0t} is consistent with the scheme shown in Fig. 7. Based on this, the longitudinal normalized RMS emittance is set to 0.3 [π mm mrad], which falls in the non-resonance region of the Hofmann chart. Subsequently, the number of proton particles was set to 100,000, the transverse particle distribution was based on *K-V*, and the longitudinal particle distribution was based on three Gaussian standard deviations. The simulation results obtained using TraceWin are shown in Fig. 8.

From Fig. 8, we can see that ε increased as the tune depression decreased (the current intensity increased), regardless of which periodic element was used. For the element that provides focusing strength by the quadrupole lattice, ε exhibits a large increase when tune depression was equal to 0.6. There are two reasons for the increase in ε: one is the influence of the space charge, and the other is the nonlinear influence of the accelerating field. Under the action of a non-linear force, particles with larger amplitude will feel a much stronger force, which makes them deviate from the law of harmonic oscillatory motion that leads to an increase in beam emittance. As the beams are focused by the solenoid lattices, ε increases slightly.

Compared to the results obtained by the 2D simulation, ε is mostly consistent. This means that the results obtained by the 2D simulation can be extended to 3D simulations. However, there are some differences. When the tune depression was equal to 0.6, ε was larger under focusing

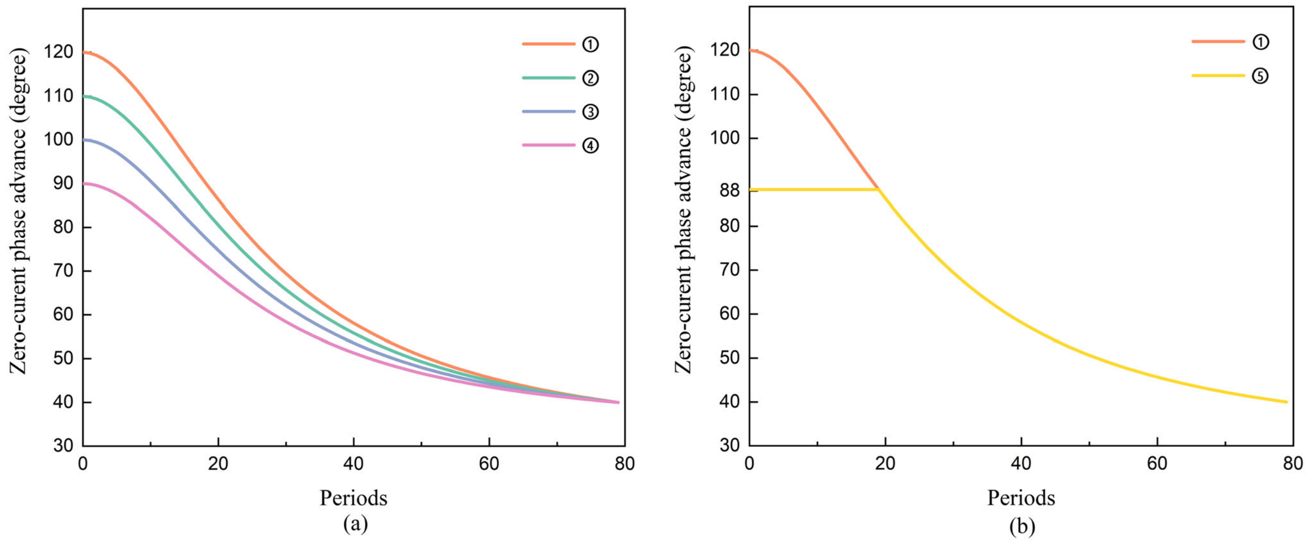

Fig. 7 (Color online) σ_{0t} for the five schemes. **a** Shows the focusing schemes ① –④ and **b** shows the focusing schemes ① and ⑤

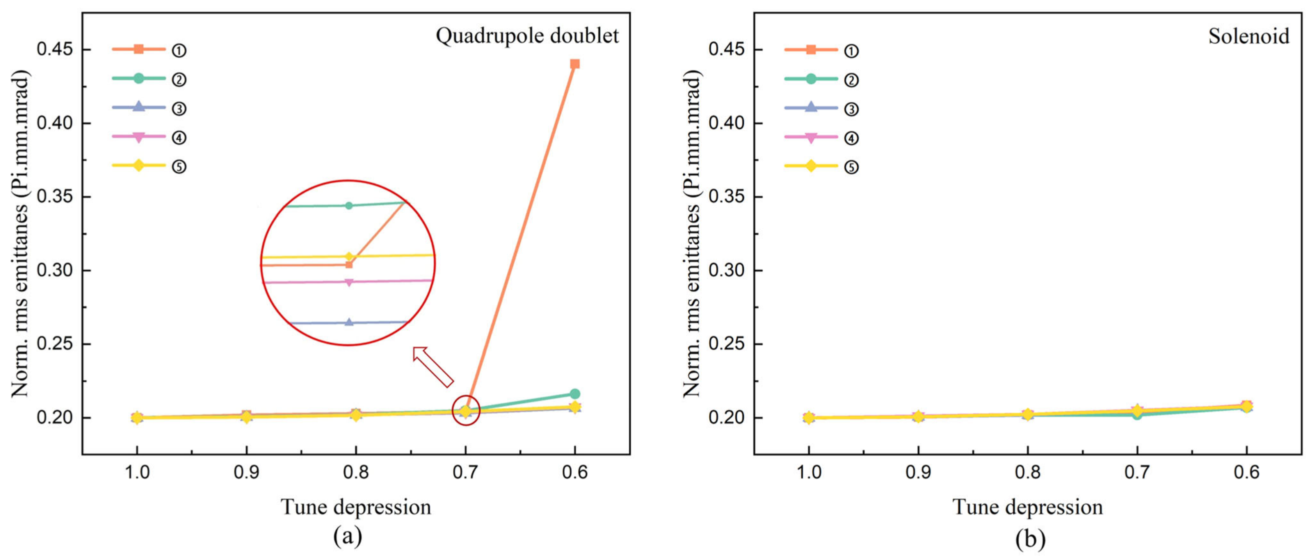

Fig. 8 (Color online) ε during beam transport. **a** Shows ε when beams were focused by quadrupole lattices and **b** shows ε when beams were focused by solenoid lattices. Different serial numbers correspond to different focusing schemes in Table 1

scheme ①. Based on this phenomenon, we separately analyzed the beam evolution under focusing schemes ① and ②. Figure 9 shows the corresponding particle distribution diagrams when the beam passed through the 9th, 24th, and 80th periods. When σ_{0t} was changed according to focusing scheme ①, the distribution of particles in the phase space had a typical four-fold structure, and filamentation occurs, but the beam core maintained a four-fold structure within a certain number of periods. Finally, the bunch was transported in the acceleration channel in an unstable structure. Therefore, in this case, the increase in the beam emittance results from the fourth-order resonance and envelope instability. This result was consistent with our conclusions. When σ_{0t} was changed according to focusing scheme ②, the distribution of particles in the phase space demonstrated a slight filamentation, but this stabilizes as the beam is transported.

6 Conclusion

In this study, we analyzed the beam dynamics when σ_0 partially exceeded 90°. Under the condition of equipartition, we used the logistic function to fit σ_0 under acceleration and then calculated the stopband with a non-constant σ. From the simulation of the beam's transverse motion, it

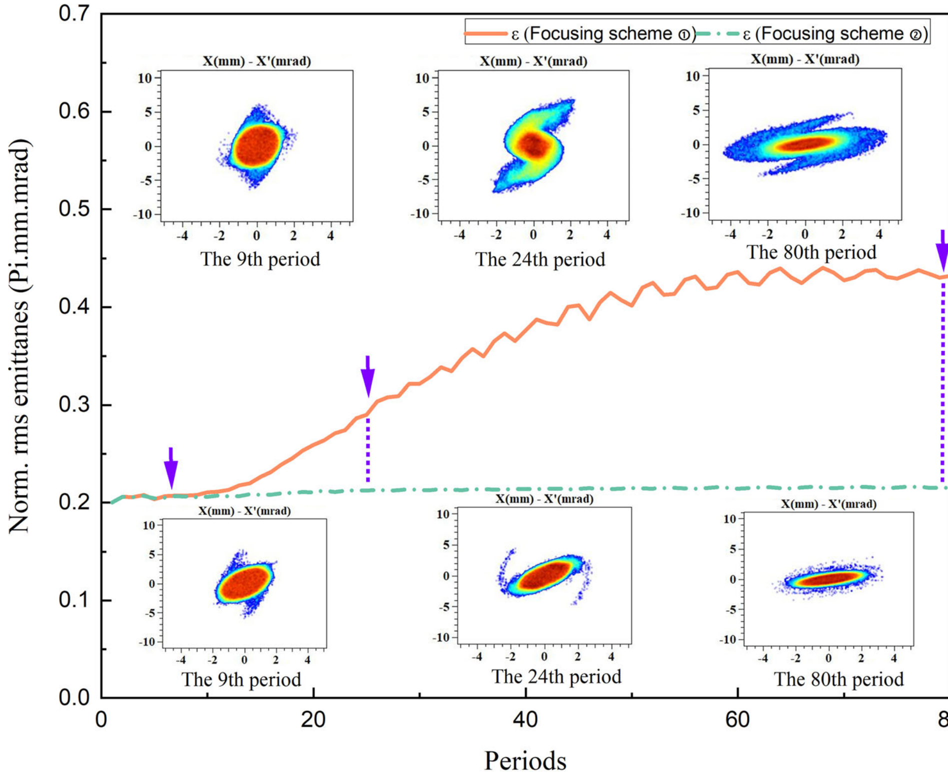

Fig. 9 (Color online) ε of focusing schemes ① and ② and the phase space distribution evolution along an acceleration channel that provides focusing strength by quadrupole doublet lattice (shown in (b) of Fig. 6) when the tune depression was equal to 0.6. Here, the particle distribution diagrams of the 9th, 24th and 80th periods are shown

is clear that the beam quality is affected by the focusing scheme, tune depression, and periodic focusing channel. By comparing the time at which the beam crosses the stopband and analyzing the particle distribution in the phase space, we concluded that when the tune depression was ≤ 0.7, the beam quality was significantly affected by the space charge. Furthermore, when σ_{0t} partially exceeded 90°, the emittance of the beam transported in the quadrupole doublet focusing channel increased significantly, which is inseparable from the superposition of the oscillation modes in this focusing structure. When the maximum σ_{0t} was 120°, the distribution of the particles in the phase space exhibited an obvious fourth-fold structure over a long period of time. In addition, the main reasons for the increase in emittance are the fourth-order resonance and envelope instability. Of course, higher-order instability also affects the beam quality to a certain extent. However, for the solenoid focusing system, there was no significant increase in the emittance under the same conditions. When Tune depression was greater than 0.7, the periodic focusing structure type and focusing scheme demonstrated little effect on the beam quality. We then simulated the beam dynamics while considering acceleration. Beams are focused on solenoid lattices, which seem to have result in high beam quality. However, beams focused on quadrupole doublet lattices show different results. When the tune depression was 0.6, ε reaches its maximum value. This is mainly due to the envelope instability and nonlinear forces in the longitudinal phase space. By comparing the results obtained from the 2D simulation with those obtained in 3D, we find that they are highly consistent. Therefore, the results obtained from 2D simulations can be extended to 3D simulations.

Author Contributions Xin-Miao Wan and Zhi-Hui Li contributed to the study conception and design. Material preparation, data collection and analysis were performed by Xue-Jiang Pu, Wei-Hong Huang, Yu-Fei Yang Xin-Miao Wan and Zhi-Qiang Ren. The first draft of the manuscript was written by Xin-Miao Wan and Zhi-Hui Li. All authors commented on previous versions of the manuscript.

References

1. J.Y. Liu, J.R. Shi, H. Zha et al., Analytic RF design of a linear accelerator with a SLED-I type RF pulse compressor. Nucl. Sci. Tech. **31**, 107 (2020). https://doi.org/10.1007/s41365-020-00815-5
2. X.L. Lu, Y. Zhang, J.R. Wang et al., Transport characteristics of space charge-dominated multi-species deuterium beam in electrostatic low-energy beam line. Nucl. Sci. Tech. **29**, 51 (2018). https://doi.org/10.1007/s41365-018-0384
3. J. Qiang, Bunched beam envelope instability in a periodic focusing channel. J. Phys: Conf. Ser **1067**, 062015 (2018). https://doi.org/10.1088/1742-6596/1067/6/062015
4. H.Y. Li, X.M. Wan, W. Chen et al., Optimization of the S-band side-coupled cavities for proton acceleration. Nucl. Sci. Tech. **31**, 23 (2020). https://doi.org/10.1007/s41365-020-0735-7

5. I. Hofmann, L. Laslett, L. Smith et al., Stability of the kapchinskij-vladimirskij (k-v) distribution in long periodic transport systems. Part. Accel **13**, 145–178 (1982)
6. T. Wangler, F. Merrill, L. Rybarcyk et al., Space charge in proton linacs. AIP Conf. Pro **448**, 3–14 (1998). https://doi.org/10.1063/1.56764
7. Z.H. Li, P. Cheng, H.P. Geng et al., Physics design of an accelerator for an accelerator-driven subcritical system. Phys. Rev. ST Accel. Beams **16**, 080101 (2013). https://doi.org/10.1103/PhysRevSTAB.16.080101
8. D.O. Jeon, Classification of space-charge resonances and instabilities in high-intensity linear accelerators. J. Korean Phys. Soc **72**, 1523–1530 (2018). https://doi.org/10.3938/jkps.72.1523
9. R.A. Jameson, Beam-intensity limitations in linear accelerators. IEEE T. Nucl. Sci **28**, 2408–2412 (1981). https://doi.org/10.1109/TNS.1981.4331708
10. C. Li, Q. Qin, R.A. Jameson et al., Space Charge Induced Collective Modes and Beam Halo in Periodic Channels. Paper Presented at the 7th Int. Particle Accelerator Conf. (IPAC'16), Busan, Korea, 8–13 May, 2016
11. J. Struckmeier, M. Reiser, Theoretical studies of envelope oscillations and instabilities of mismatched intense charged particle beams in periodic focusing channels. Part. Accel **14**, 227–260 (1983)
12. M. Chung, Y.L. Cheon, H. Qin, Linear beam stability in periodic focusing systems: Krein signature and band structure. Nucl. Instrum. Meth. A **962**, 163708 (2020). https://doi.org/10.1016/j.nima.2020.163708
13. X.Q. Yan, R.A. Jameson, Y. Lu et al., Matched and equipartitioned design method for modern high-intensity radio frequency quadrupole accelerators. Nucl. Instrum. Meth. A **577**, 402–408 (2007). https://doi.org/10.1016/j.nima.2007.03.031
14. R.A. Jameson, An approach to fundamental study of beam loss minimization. Paper Presented at the AIP Conference Proceedings. American Institute of Physics, vol. 480, pp. 21–30 (1999). https://doi.org/10.1063/1.59501
15. P. Paul, G. Sprouse, Superconducting linear accelerators for heavy ions. Comments Nucl. Particle Phys. **11**, 217–229 (1983)
16. G. Geschonke, Superconducting structures for high intensity linac applications, in *Proceedings of the XVIII International Linear Accelerator Conference*, 8 October 1996. pp. 910–914. https://doi.org/10.5170/CERN-1996-007.910
17. M. Weiss, Radio-frequency quadrupole, in *5th Advanced Accelerator Physics Course*. pp. 959–991 (1995). https://doi.org/10.5170/CERN-1995-006.959
18. D.O. Jeon, J. Jang, H. Jin, Interplay of space-charge fourth order resonance and envelope instability. Nucl. Instrum. Meth. A **832**, 43–50 (2016). https://doi.org/10.1016/j.nima.2016.06.036
19. F.J. Sacherer, Rms envelope equations with space charge. IEEE T. Nucl. Sci **18**, 1105–1107 (1971). https://doi.org/10.1109/TNS.1971.4326293
20. D. Chernin, Evolution of rms beam envelopes in transport systems with linear x–y coupling. Part. Accel **24**, 29–44 (1988)
21. C. Li, R.A. Jameson, Structure resonances due to space charge in periodic focusing channels. Phys. Rev. Accel. Beams **21**, 024204 (2018). https://doi.org/10.1103/PhysRevAccelBeams.21.024204
22. Wolfram mathematica, URL http://www.wolfram.com/mathematica/. Accessed 9 Jul 2022.
23. TraceWin, URL http://irfu.cea.fr/dacm/en/logiciels. Accessed 9 Jul 2022.
24. T. Wangler, K. Crandall, R. Ryne et al., Particle-core model for transverse dynamics of beam halo. Phys. Rev. Accel. Beams **1**, 084201 (1998). https://doi.org/10.1103/PhysRevSTAB.1.084201
25. Y.S. Yuan, O. Boine-Frankenheim, I. Hofmann, Modeling of second order space charge driven coherent sum and difference instabilities. Phys. Rev. Accel. Beams **20**, 104201 (2017). https://doi.org/10.1103/PhysRevAccelBeams.20.104201
26. Y. Cheon, S. Moon, M. Chung et al., Analysis on the stop band of fourth-order resonance in high-intensity linear accelerators. Phys. Plasmas **27**, 063105 (2020). https://doi.org/10.1063/5.0004651
27. R.A. Jameson, Equipartitioning in linear accelerators. Los Alamos National Laboratory (Report) LA, Santa Fe, NM, USA, 19 October 1981